Journal of Solid State Electrochemistry (2024) 28:965–979
https://doi.org/10.1007/s10008-023-05381-5

FEATURE ARTICLE

An experimental guide to *in operando* electrochemical Raman spectroscopy

Thorben Lenk[1,3] · **Uwe Schröder**[2,3]

Received: 24 November 2022 / Revised: 3 January 2023 / Accepted: 3 January 2023 / Published online: 17 January 2023

Abstract

Electrochemical Raman spectroscopy can provide valuable insights into electrochemical reaction mechanisms. However, it also shows various pitfalls and challenges. This paper gives an overview of the necessary theoretical background, crucial practical considerations for successful measurement, and guidance for in situ/*in operando* electrochemical Raman spectroscopy. Several parameters must be optimized for suitable reaction and measurement conditions. From the experimental side, considerations for the setup, suitable signal enhancement methods, choice of material, laser, and objective lens are discussed. Different interface phenomena are reviewed in the context of data interpretation and evaluation.

Keywords Spectroelectrochemistry · Raman spectroscopy · Tutorial · SERS · Vibrational spectroscopy

Introduction

With a growing interest in electrochemical processes comes an increasing attentiveness to in situ and *in operando* methods that can provide further insight into reaction mechanisms and the behavior of the involved substances on a molecular scale. A clear differentiation of both terms is often difficult, leading to an interchanged use.[1] While techniques like XRD (x-ray diffraction) and LP-TEM (liquid-phase transmission electron microscopy) are suitable tools for investigating the crystal structure and morphology of solid-state electrodes, SECM (scanning electrochemical microscopy) can provide information on the electrochemically active species in the liquid phase [1]. The information that these techniques cannot provide is information on the surface species from the liquid side. In situ Raman and IR spectroscopy can fill this gap and allow investigating the molecular situation close to the surface, e.g., adsorbates, binding situations, molecular orientations, changes during a reaction, and intermediates [2–4]. These vibrational spectroscopic techniques are frequently employed for in situ/*in operando* investigations of catalytic processes [4–7]. Besides advantages like high temporal and spectral resolutions and sensitivities [3], the weak water signals make Raman spectroscopy an ideal tool for the in situ/*in operando* investigation of aqueous electrochemical reactions. Several Raman spectroelectrochemical studies have improved the understanding of electroorganic synthesis [7–11], electrocatalysis [12, 13], batteries [14], electrode interface behavior [15], and material science [16]. Also, molecule/surface interactions without applied potentials can be examined [17]. The interdisciplinary topic of electrochemical Raman spectroscopy is positioned at the interface of electrochemistry, spectroscopy, catalysis, nanomaterial and surface science, optics, and experimental physics.

✉ Uwe Schröder
uwe.schroeder@uni-greifswald.de

[1] Institute of Environmental and Sustainable Chemistry, Technische Universität Braunschweig, Braunschweig, Germany

[2] Institute of Biochemistry, University of Greifswald, Greifswald, Germany

[3] Cluster of Excellence SE2A-Sustainable and Energy-Efficient Aviation, Technische Universität Braunschweig, Braunschweig, Germany

[1] Both terms describe a usually spectroscopic investigation of a certain reaction or of the involved chemical species within the experimental environment. While *in operando* is a more strict attribute to a spectroscopic investigation of a reaction under working conditions, the definition of in situ is broader, including experiments that do not fulfill the target reaction conditions (for example a high pressure or a high temperature as typical for e.g., heterogeneous catalysis) for an *in operando* method [76]. As electrochemical reactions typically proceed under milder ambient reaction conditions [77], they are in many cases easier to investigate under more ideal *in operando* conditions. In this context, we understand the term "spectroelectrochemistry" as an *in operando* utilization of spectroscopic techniques for the study of electrochemical processes.

This paper is addressed to readers new to the field as a guide towards their first electrochemical Raman spectroscopic experiments. It aims to combine knowledge from the involved sub-disciplines to better understand suitable conditions for Raman spectroscopy as a method to examine electrochemical processes under reaction conditions. Hereby, the paper gives an overview of crucial experimental parameters, including the spectroelectrochemical setup, objective lenses, and the choice of the appropriate laser—by means of exemplary measurements using selected model systems. A special focus is put on possibilities to analyze molecular species close to electrode surfaces by surface-enhanced Raman spectroscopy (SERS). Furthermore, processes interfering on a molecular scale will be summarized to understand necessary considerations for data evaluation.

The consideration of solid-state electrochemical reactions, e.g., of active materials in lithium ion batteries, is outside the focus of this paper, since special aspects such as an anhydrous atmosphere have to be taken into account here. The reader is therefore referred to the respective literature [18].

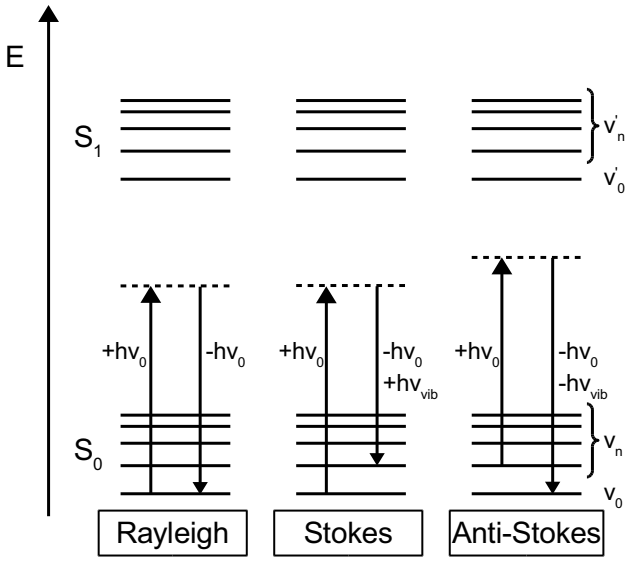

Fig. 1 Energy diagram depicting the processes of elastically (Rayleigh) and inelastically (Stokes and Anti-Stokes) scattered light. Dashed lines: virtual states, Solid lines: actual states

Fundamentals of Raman spectroscopy

In 1928, C.V. Raman found that upon illumination of a material with a monochromatic light source, light shifted to longer wavelengths could be detected besides radiation of the incident wavelength. In some cases, he also observed shifts to shorter wavelengths [19]. In 1930, the finding of the Raman effect was rewarded with a Nobel prize in physics and was the starting point for Raman spectroscopy. His observations can be explained by viewing Fig. 1.

An incident light beam is directed to a material and consequently scattered in all directions. There are three different scattering mechanisms [20]. The majority of photons scattered at the material experience elastic scattering [21]. This scattering without a loss in energy is called Rayleigh scattering. This means the molecule absorbs radiation of the energy E_0 from the light source, which excites the molecule into a virtual state. For an excitation into an actual excited state S_1, the energy of the E_0 is too low. The virtual state is unstable and immediately leads to light emissions with the same energy. One out of 10^8 photons of the radiation scatters inelastically [21]. One variant for this is the Stokes scattering. Here, the light emitted from the molecule has less energy as the molecule is going into an excited vibrational state. The molecule has more energy than in the ground state, while backscattered light has less energy, leading to higher wavelengths [20]. The opposite happens for anti-Stokes scattering. The molecule is already in an excited vibrational state due to Boltzmann distribution and relaxes into the vibrational ground state [22]. Here, the emitted light has a lower wavelength, hence more energy than the incident radiation [20]. While Rayleigh scattering is not useful for spectroscopic measurements, Stokes and anti-Stokes scattering provide information on the molecule's vibrations and, thereby, on the binding situation and moieties of the molecule. Under ambient conditions, the vibrational ground state is the most populated, so statistically, Stokes scattering has a higher chance of occurring. Only one molecule of a million Raman scattering molecules is in an excited state, resulting in anti-Stokes scattering [22]. Hence, the term Raman spectroscopy is typically used for spectroscopy under evaluation of the Stokes-scattering, while anti-Stokes Raman spectroscopy is a more specialized technique, e.g., in Coherent anti-Stokes Raman Spectroscopy (CARS) [20, 23]. The difference between the incident light's wavenumber and measured inelastically scattered radiation gives the Raman shift. It usually covers a wave number range between ca. 50 and 3500 cm^{-1}, with organic compounds usually to be found in the mid-IR, whereas the Raman shifts of solid inorganic compounds can also reach into the far-IR (below 400 cm^{-1}). Thus, vibrational excitations in the energy range of infrared light are evaluated by applying a more energetic radiation like ultraviolet (UV) or visible light (Vis). Conventional IR transmission or absorption spectroscopy also examines molecular vibrations, however, by using IR illumination/excitation. Although both Raman and IR spectroscopy display molecular vibrations, the resulting spectra, and the conditions differ and represent the two counterparts of vibrational spectroscopy. Of all the 3 N-5, respectively 3 N-6 possible vibrations of a molecule with N atoms, not each vibration is active in IR and Raman spectroscopy. IR

spectroscopy requires a change in dipole moment during a vibration, while Raman spectroscopy is based on changing the polarizabilities of the molecule [24]. These selection rules lead to different vibrations being either only Raman or IR active, while others are active in both techniques but with different intensities. Usually, a decision on whether a vibration is active or not requires a deeper investigation of its symmetry or an application of group theory. For a more detailed understanding of the theoretical background, the reader is referred to the literature [20, 22, 24, 25].

Raman spectroscopy possesses several advantages over IR spectroscopy in its application for spectroelectrochemical experiments [26]. One of the disadvantages of IR spectroscopy is the severe absorption of infrared radiation by water leading to the limited applicability of this technique in spectroelectrochemical measurements in aqueous solutions. In contrast, Raman spectroscopy is barely affected by water as a solvent [2, 3]. Furthermore, the applied optical setup is important. IR spectroscopy requires optical windows made of IR-transparent materials such as KBr, making it difficult to process and handle in aqueous electrochemical cells. Their usage can be avoided by applying attenuated total reflection (ATR) IR spectrometers [24, 27] that require potentially complex electrode preparation methods, and that can be limited with respect to the used electrode materials. Respective studies typically employ SEIRAS (surface-enhanced infrared absorption spectroscopy) [28–31]. Meanwhile, Raman spectra can be measured through conventional quartz or sapphire glass, as the light source and detected light is in the range of UV/Vis [25].

Typical spectroscopic setups

The first Raman spectrometers were built in a 90° geometry in analogy to the comparable fluorescence spectrometers. Here, the 90° geometry aids in minimizing the amount of non-scattered photons, reducing the comparably large Rayleigh scattering signal at a Raman shift of 0 cm^{-1} when no filters or laser light sources were available. As light is scattered in all directions, there is, in principle, no preferred direction to measure the resulting spectrum. Also, 0° geometries are possible with the detector being in one line with the light source and the sample. In the last decades, microspectroscopy with a 180° geometry gained interest in creating composition images by mapping surfaces and volumes, as a piezoelectric positioning system allows for a non-invasive lateral and depth scanning of analytes [32]. Most current in situ setups employ this 180° backscattering geometry (Fig. 2), in which the laser beam is pointed perpendicular to the electrode surface before the resulting backscattered light is collected with the same optics and subsequently brought to the detector [4]. This experimental

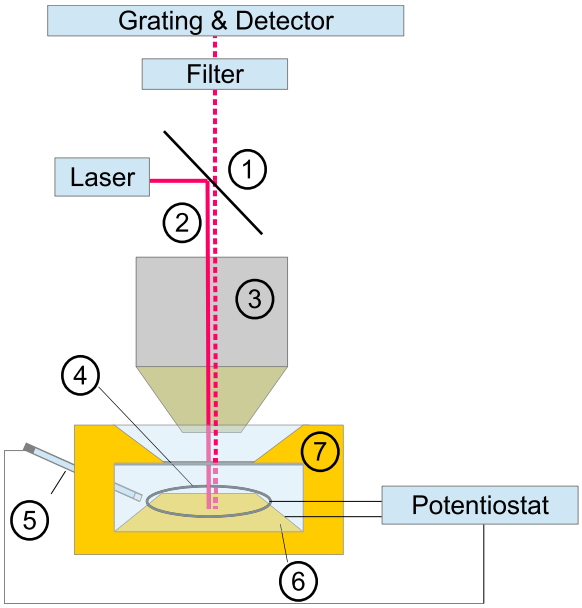

Fig. 2 Typical setup of a spectroelectrochemical Raman cell in a Raman microscope with 180° backscattering geometry with (1) dichroic mirror, (2) laser beam and scattered light, (3) objective, (4) counter electrode, (5) reference electrode, (6) working electrode, and (7) spectroelectrochemical cell

configuration, combined with a curled wire or a metal foil with a hole for the radiation beam as a counter electrode, enables the electrochemist to investigate the side of the working electrode facing the counter electrode. In *in operando* cells, the backscattering setup of microspectroscopes allows a convenient optical pathway and the possibility to measure confocally, only obtaining spectroscopic information from the focused area [33]. For heterogenic electrodes, a differentiation between morphological and constitutional areas is also possible.

The typical components of a spectroelectrochemical Raman experiment are illustrated in Fig. 2. An essential part of it is the laser. It is necessary as a light source to efficiently generate monochromatic light with high intensity. Before lasers were commercially available, Raman spectrometers could only employ less intense light sources, leading to a considerable effort in signal detection and analytical limitations. Applying modern lasers with higher intensities helped Raman spectroscopy overcome its niche status and increase its exploitability. The laser beam is reflected at a dichroic mirror, bringing the light through an objective to the sample, where the laser light is focused and scattered. The objective also collects the scattered light and brings it to the dichroic mirror, which mainly transmits the scattered light with a lower wavenumber than the incident laser beam, which is reflected. This dichroic mirror is the first step in reducing the intensity of the Rayleigh scattering. In a second step, a notch filter blocks the light with a wave number equal to the light source from detection. For the actual detection, first,

a dispersion of wave numbers at a grating and subsequent detection with a charge-coupled device (CCD) detector is realized. While the grating provides a separation of the differently energetic wave numbers, the CCD detector provides information on the intensity of the individual wave number [32]. For a more detailed understanding of different components, their historical development, and the possible setup, the reader is referred to more detailed literature [20, 24].

Enhancement methods

The (inelastic) Raman scattering comprises an only small portion of the scattered radiation. Additionally, the concentrations of studied dissolved or adsorbed species in electrochemical experiments are generally comparatively low. For these reasons, the obtained Raman signals often exhibit a low intensity, leading to a low signal-to-noise ratio, generally weak signals and non-observable vibration bands [33]. With SERS, this issue can be addressed. Figure 3A, B show the influence of this effect on the Raman spectra. While the unroughened (here considered weakly enhanced) surfaces provide a poor spectrum quality, the roughened surfaces give a higher signal-to-noise ratio and thus the option for lower laser intensities to prevent damage to the sample and undesired sample interaction from laser irradiation. Furthermore, signals from species not adsorbed at the surface are discriminated—like, in this case, the signals from the sulfuric acid electrolyte system. Scanning electron microscopic (SEM) images of the roughened and unroughened surfaces are depicted in Fig. 4.

Tremendous effort went into the research for the optimization of substrates and application in several research fields ranging from analytical chemistry [37, 38] and nanomaterial research to evaluating biological samples [39]. For a deeper insight into the theory behind SERS and more detailed summaries, recent publications are recommended, while we provide a brief summary here [40–43]. The SERS effect first described in 1974 by Fleischmann et al. [44] as an enhancement of a pyridine signal on an electrochemically roughened Ag surface and subsequently explained by Jeanmaire et al. [45] and Albrecht et al. [46] in 1977 allows a drastic enhancement of Raman intensity with enhancement factors of 10^4–10^{14}, depending on the respective conditions [47], that exceeds the contribution of the increased surface area. This enhancement is helpful for a further investigation of the otherwise low-intense surface species and vibration bands. The SERS effect can be explained by two mechanisms. The first one, chemical enhancement, has a minor contribution. It is based on photoinduced charge transfer processes between the molecules' highest occupied molecular orbital (HOMO) and the metal's Fermi level or from the Fermi level of the metal to the lowest unoccupied molecular orbital (LUMO) of the irradiated molecule [42]. As the polarizability of the molecule can change during the charge transfer process, it can lead to changing Raman scattering cross-sections [41]. The chemical enhancement leads to an enhancement of individual vibration bands compared to the normal, unenhanced Raman spectrum. On the other hand, the second effect, plasmonic enhancement, exhibits a higher enhancement factor. It relies on localized surface plasmons.

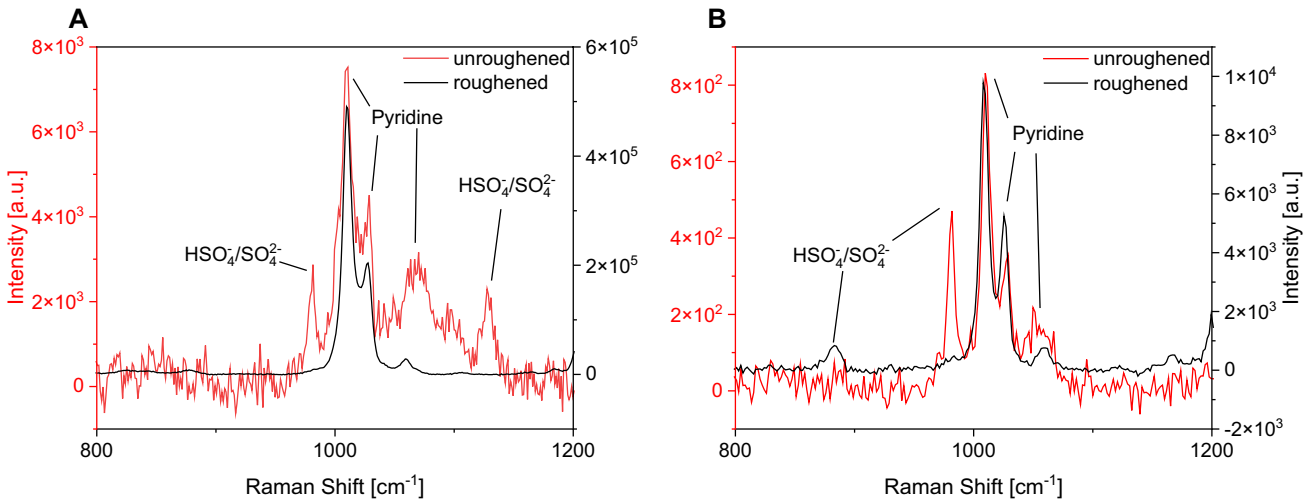

Fig. 3 Raman spectra of **A** copper surface unroughened (1 s, 100 accumulations, 100% intensity) and roughened (1 s, 25 accumulations, 10% intensity) with 785 nm laser and **B** silver surfaces unroughened (1 s, 10 accumulations, 50% intensity) and roughened (1 s, 10 accumulations, 50% intensity) with 532 nm laser; 0.1 M sulfuric acid solution and 0.05 M pyridine; alignment of the Raman signals based on literature: HSO_4^- / SO_4^{2-} [34], pyridine [35, 36]

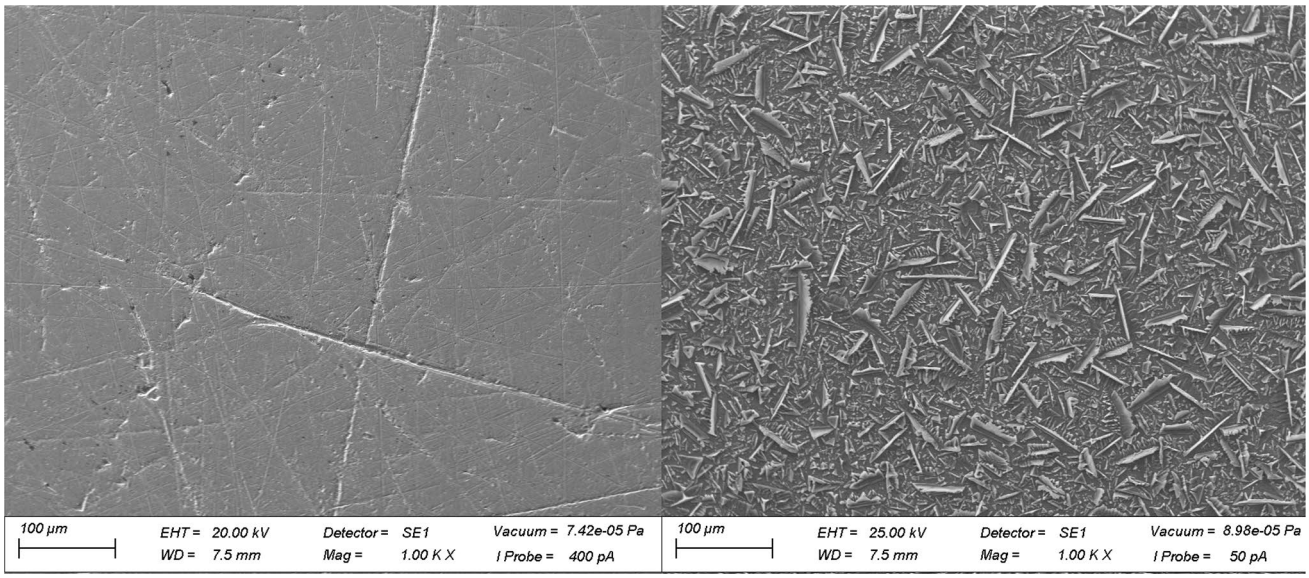

Fig. 4 SEM images of copper electrode surfaces before and after ORC

Plasmons are electron density oscillations in a small metal structure. If the wavelength of an incident light coincides with the local surface plasmon oscillation, it comes to resonance and an enhancement of the electromagnetic field of the metal structure, leading to enhanced scattering [48]. The extent of enhancement is mainly dependent on the size and shape of the formed structures [41, 49]. As the plasmonic enhancement is specific towards the direction of the enhanced vibration, Raman spectra of surface species can substantially differ from the solution spectra. Following the surface selection rules, vibrations can be completely unenhanced, moderately enhanced, or strongly enhanced depending on the molecule's orientation on the surface, although a roughened surface can influence the exact orientational angle of the molecule towards the incident light [50–52].

In the last decades, there has been tremendous interest in the preparation of optimally enhancing substrate surfaces. Most often described are methods for preparing SERS substrates of the coinage metals Ag, Au, and Cu, as they exhibit a high enhancement factor and stability of nanoparticle structures [2]. However, Ag and Au SERS substrates are preferred over Cu as Cu tends to be chemically less stable [53]. There are several different examples of substrate preparation of these metals for SERS [38, 40, 42, 53]. Other metals like Pt, Rh, Fe, and Co also exhibited a signal enhancement, although less often described due to their lower ability for enhancement [33, 54]. The application of other transition metals often comes with the utilization of UV light lasers [54]. As not all metals exhibit a substantial signal enhancement, the technique of borrowed enhancement was developed. Here, a SERS substrate, typically of Au, is prepared and covered with a thin layer of the desired surface material [55]. As the electromagnetic enhancement of the SERS substrate decreases with r^{-12} [41] to the surface, an enhancement of adsorbates is even observed if there is a cover layer between the SERS substrate and the actual analyte. In this context, r is defined as the distance between a molecule and the center of the particle it is adsorbed on. Plenty of morphologies and metal combinations are described for this strategy in the literature [55]. Similar to this approach, the shell-isolated nanoparticle-enhanced Raman spectroscopy (SHINERS) consists of uniform cores, e.g., from SiO_2, covered with a layer of coinage metal [56, 57].

Despite the large variety of methods described for preparing SERS substrates, the most important ones for spectroelectrochemistry can generally be divided into the following subgroups: electrochemical roughening, chemical nanoparticle synthesis, chemical etching, and laser techniques (Table 1) [20, 38, 53]. Electrochemical roughening procedures are typically the most convenient to employ prior to a spectroelectrochemical measurement, as they can be executed directly before the actual experiment using the same experimental setup. They typically consist of oxidation–reduction cycles (ORC), in which the metal is oxidatively dissolved before it is reductively attached to the metal surface, leading to rough unordered morphologies with differently sized and shaped features [55]. Also, the direct electrochemical reduction from respective salt solutions is described [58]. While the advantage of the electrochemical techniques lies in the convenience for spectroelectrochemical experiments, they do not yield a perfectly homogeneous surface morphology (Fig. 4) and, therefore, no reproducible signal enhancement [33]. Even the extent and quality of prior polishing of metal surfaces play a significant factor in

Table 1 Comparison of advantages and disadvantages of different procedures for SERS substrate preparation

Method	Advantage	Disadvantage
Electrochemical (e.g., ORC)	Convenient setup and preparation	Heterogeneous surface, no reproducible or exact surface/enhancement effect
Chemical NP synthesis	Simple procedure, more control over NP size	Possibility of the introduction of impurities, questionable attachment to the surface
Laser	More defined surface	Specialized equipment necessary
Chemical etching	Simple procedure	Difficult reproduction, lower enhancement
Template method	Highly ordered structures	Challenging electric contact

different performances of SERS substrates, as the resonance of the laser with the surface plasmon requires a specific nanoparticle size for maximal enhancement. For chemical nanoparticle (NP) synthesis, the size distribution and, therefore, the Raman signal enhancement is easier to adjust and controllable by temperature and reaction time [59]. However, potentially utilized reducing agents and tensides may cause contamination of the Raman spectra with undesired remaining chemicals [53]. Furthermore, the durability of the NP attachment to the surface might be insufficient. Another major SERS preparation method involves laser ablation techniques. This technique requires specialized equipment but produces well-defined surface structures in a reproducible manner [53]. Other methods include chemical etching [60], which is easily performed but often lacks satisfying enhancement factors [2, 61]. Most mentioned techniques provide an array of NP sizes and distributions leading to non-uniform enhancement factors. On the other hand, template methods produce highly ordered substrates while providing sufficient electric contact is challenging [62].

Substrate and wavelengths

Besides the SERS substrate, laser light has an important influence on the measurement. When looking for an appropriate choice for the laser wavelength, one has to consider the desired substrate material. Figure 5 shows the signal intensity and signal-to-noise ratio dependence on the employed laser in combination with the utilized metal surface. A 785 nm laser, utilized with a copper electrode material, gives a more than 132 × more intense signal along with a significantly better signal-to-noise ratio than a 532 nm laser under otherwise similar conditions. On the other hand, a silver electrode material shows a more intense signal with a better signal-to-noise ratio with a 532 nm laser than with a 785 nm laser of comparable intensity. The origin of this observation is the different maxima of the surface plasmon resonance of the substrate materials. While the maximum of copper or gold is more in the near-IR range, silver possesses a maximum at a more energetic wavelength at ca. 600 nm [63]. Although the size and shape of the utilized nanoparticles also influence the maximum position [41], optimization is challenging due to the heterogeneous substrate utilized. The closer the laser wavelength is to the maximum of the plasmon resonance, the higher will be the enhancement of the Raman signal. Figure 5A, B also show different signals stemming from enhanced signals of surface species (Fig. 5B), while the copper surface species in (Fig. 5A) is not enhanced, leading to typical solution spectra of pyridine spectra from the adjacent volume within the spatial resolution (see section "Choosing the right objective"). Silver in Fig. 5D, on the other hand, is still enhanced, although the laser light is not at the plasmon resonance maximum, leading to a lower signal intensity despite revealing vibration bands of the surface species. These experiments show that not every laser is suitable for each experiment. Hence, if an optimal laser for every desired plasmonic material is too costly, finding lasers that provide the best compromise between the wavelengths may be advantageous. Other general considerations for applied lasers include higher excitation efficiency and lower heat adsorption for lower wavelengths [20]. On the other hand, lower wavelengths also show a higher tendency for fluorescence [20].

Besides the laser wavelength, its intensity, number of accumulations, and acquisition time play a crucial role in acquiring spectra. The higher the laser intensity, the number of accumulations, and the longer the acquisition time, the higher the possible Raman scattering intensity and signal-to-noise ratio.

Choosing the right objective

Typical EC Raman experiments employ a confocal Raman microscope. A confocal aperture blocks light originating from outside the point focused with the microscope's optics [64]. It allows differentiation between signals from different positions under a variation of three positionable axes to change the proximity to the electrode and the position on the surface. This way, it is expected only to examine signals from the desired area. Unfortunately, the application of Raman

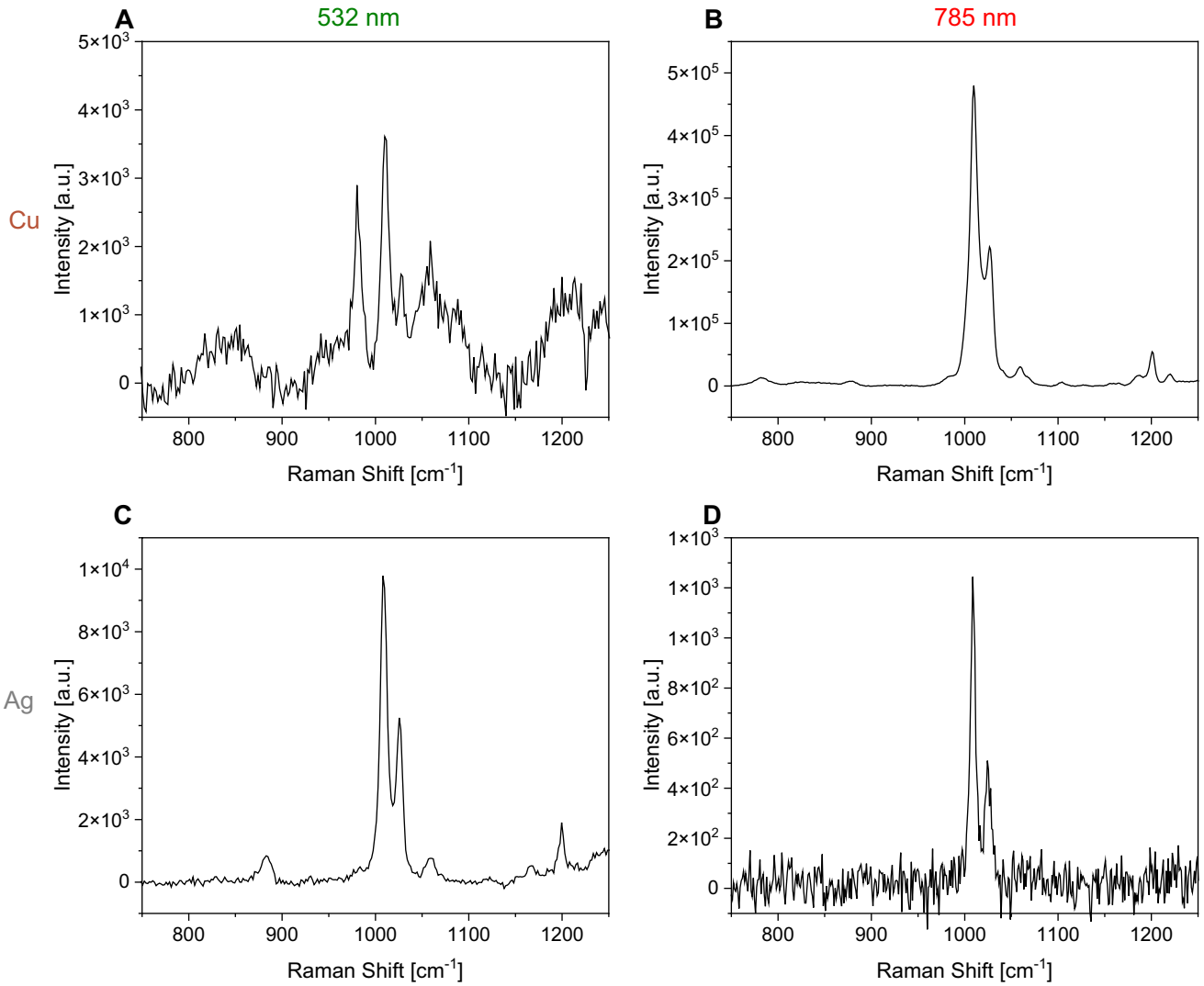

Fig. 5 Comparison of the four combinations arising from the use of either copper or silver surfaces and the use of either a 532 nm or a 785 nm laser on the Raman spectra of 0.05 M pyridine in 0.1 M sulfuric acid solution. **A** Copper with a 532 nm laser (1 s, 25 accumulations, 50% intensity). **B** Copper with a 785 nm laser (1 s, 25 accumulations, 10% intensity). **C** Silver with a 532 nm laser (1 s, 10 accumulations, 50% intensity). **D** Silver with a 785 nm laser (1 s, 10 accumulations, 10% intensity)

spectroscopy in electrochemistry requires more consideration here. Numerous publications reporting electrochemical Raman spectroscopy do not specify the objective lens attached to the spectrometer or use a non-ideal metallurgical objective making it challenging to choose the right objective. Since commercial Raman microscopes are typically delivered with metallurgical objectives, this appears to be a suitable first choice—although it is easy to avoid this obstacle [65].

Figure 6 shows the intensity of the pyridine ring breathing mode [66] at 1008.5 cm^{-1} in a 0.05 M aqueous solution with varying distances z to the metal surface using two different kinds of objectives (see Fig. 7A, B). In both cases, the sapphire surface (i.e., the transparent lid of the spectro-electrochemical cell) was focused, representing a distance to the surface of $z = 0$ µm. Positive distances mean the focus moves into the gap between the electrochemical cell and the objective, while negative distances shift into the solution. The actual distance between the sapphire surface and the electrode surface inside the electrochemical cell is 3250 µm. As pyridine is adsorbed at the surface and the SERS effect shows the maximal enhancement near the surface, a higher intensity of the Raman signal would be expected at $z = -3250$ µm. However, the metallurgical objective (5×, 0.12 NA) shows the maximum pyridine signal intensity at $z \approx -2390$ µm. In contrast, the water immersion objective (20×, 0.5 NA) exhibited its maximum at a distance to the sapphire surface of $z = -3200$ µm.

This discrepancy between metallurgical and immersion objectives derives from the different refractive indices n of the involved transparent media. While air ($n \approx 1$) has a

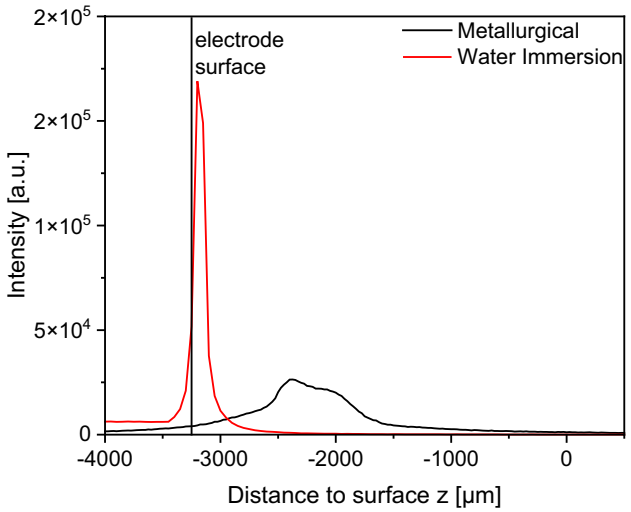

Fig. 6 Plot of pyridine ring breathing mode signal intensity [66] at 1008.5 cm^{-1} vs. the distance to the focussed sapphire surface. Negative distances move towards the copper surface, positive towards the sapphire-objective gap. Sapphire at $z = 0$

relatively low refractive index, the values of water ($n = 1.333$) and sapphire ($n = 1.761–1.769$) are higher [67]. The laser beam and backscattered light must cross the electrolyte for all possible optical setups (Fig. 7). The light's pathway goes only for the metallurgical objective through air. Metallurgical objectives, however, are designed for imaging opaque surfaces without light being partially transmitted through an optically denser environment like water [65]. This way, metallurgical objectives lead to a series of disadvantages for in situ electrochemical Raman spectroscopy. First, distances within aqueous solutions appear shorter than in air as a distance of z is already exceeded after $z_{metallurgical} = z/n$ [65]. In the example in Fig. 6, this means that although the distance is $z = -3250$ µm, it theoretically appears after $z_{metallurgical} = -3250$ µm / 1.33336 = 2437 µm, which is comparable to the experimentally obtained − 2390 µm. The even higher refractive index of sapphire was not considered here but also contributes to the mismatching distances for both objectives with a slight shift of ≈ 50 µm. Hence, performing a Raman spectroscopic analysis of, e.g., an intensity profile will not give the actual distances. Avoiding depth measurements and simply focusing on the surface for a Raman spectrum will bring the maximum intensity for the setup, but still, only a small amount of signal intensity is attenuated. A direct comparison of a water immersion objective (with a typically higher NA) with a metallurgical objective (with typically lower numerical aperture (NA)) as in our example is biased, as the different NA lead to different depth resolutions as well. However, the general behavior remains as described. The influence of the NA of an objective is described below in more detail.

Secondly, a comparison of the graphs in Fig. 6 reveals different heights and widths of the respective graphs. The water immersion objective shows a higher maximum intensity and a narrower depth array with high intensities. Again, metallurgical objectives are shown to be not ideal for this task, while water immersion objectives are intended for this application. For a deeper understanding, the reader is referred to literature while we provide a summary [65, 68, 69].

In metallurgical objectives, spherical aberration occurs. The depth resolution deteriorates since rays refracted at the surface of the objective are focused at a larger distance leading to a larger area where the signal derives from [65]. Additionally, the issue of shorter distances mentioned above is enlarged, and the array the signal derives from is broader than with shorter pathways through the water. All this leads to an unnecessarily deteriorated spatial resolution. Furthermore, increasing depths in water result in an attenuation of the Raman signal as a blurred laser leads to a blocking of parts of the radiation and less laser light focused at the intended position and, therefore, less Raman scattering. Aqueous solutions are also better radiation absorbers, generating additional signal attenuation with more depth [65]. Spherical aberrations and blurred lasers not only lead to less signal intensity but also to enhanced mixing of species' signals that were not originally intended to be in focus.

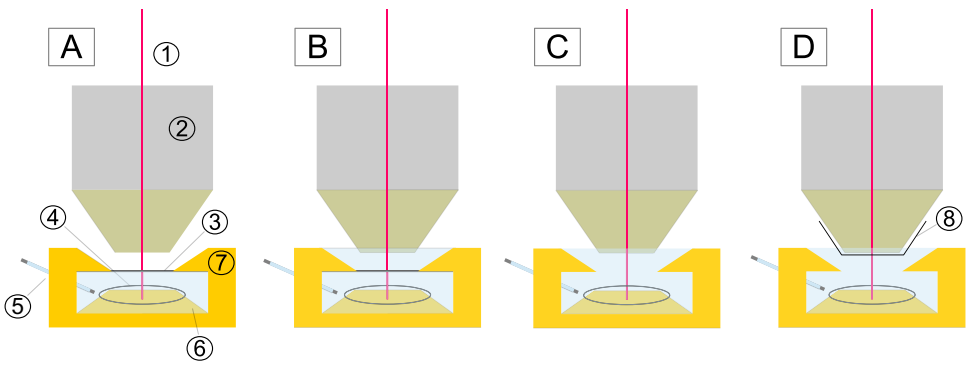

Fig. 7 Possible optical setups using **A** a metallurgical objective, **B** a water immersion objective with a sapphire window, **C** a water immersion objective without a sapphire window, and **D** a water immersion objective without a sapphire window but a protective PVC foil. (1) Laser beam, (2) metallurgical/water immersion objective, (3) sapphire window, (4) coiled counter electrode, (5) reference electrode, (6) working electrode/SERS substrate, (7) spectroelectrochemical cell, and (8) protective PVC foil

Depending on the desired kind of investigation, this might be an obstacle. Metallurgical objectives' weaknesses can be significantly overcome by utilizing a water immersion objective since it is designed for measuring through water and therefore operate with less aberration, attenuation, and correct distances [65]. Some groups suggest small solution layer thicknesses to avert significant signal losses for metallurgical objectives [33]. This decision is controversial since setups with small solution layers are prone to ohmic drop and uneven electric field phenomena, and a faster educt depletion [70]. Water immersion objectives can easily avoid these difficulties with larger solution layer thicknesses and the resulting problems.

Another possibility for the optical setup is simply avoiding a sapphire window for a more satisfying depth accuracy and higher signal intensities. Omitting the sapphire window also enables the utilization of objectives with lower working distances than the cell design allows, giving the opportunity to use objectives with higher magnifications. Additionally, Tian et al. state that lower working distances are followed by less attenuation of the Raman signal intensity as the electrolyte layer is damping the signal less [33]. However, the attenuated signal intensity for long distances in an electrolyte layer only plays a significant role for metallurgical objectives [65]. A more significant impact has the NA, which is typically higher for higher magnifications and lower working distances. It can be calculated using $NA = n \sin(\theta)$, with the angle θ being half of the opening angle of the objective. It describes the area a scattered photon can find its way from to the objective. With higher angles, a larger area of the samples is covered. Hence more photons from the area, scattered in different directions, reach the detector through the objective leading to higher signal intensity [33]. Additionally, a higher spatial resolution is possible since the laser can be focused on a smaller spot [65].

Figure 7C, D depict two alternative setups for the use of water immersion objectives. Figure 7C directly immerses the objective into the electrolyte solution. Thereby, any optical influences by other media are eliminated. For electrochemical experiments, two considerations are important here. First, the objective should not have an electrically conductive part in the solution to avoid interferences with the measurement. For this purpose, commercial water immersion objectives with ceramic fronts are available. Secondly, for all employed water immersion objectives, the chemical resistance of the surface in contact with the electrolyte should be considered. Many electrolytes enable the corrosion of metals or dilution of metals and oxides, leading to a shortened lifetime of objectives [33]. Figure 7D shows an adapted setup most often described by Tian et al. [2, 33]. In their work, they describe the protection of a metallurgical objective from corrosion with a thin foil of polyvinyl chloride (PVC). Attached to a water immersion objective, this allows the objective to be immersed into corrosive electrolytes, enabling lower working distances, a higher NA, and fewer influences by window materials. Possibly emerging gas bubbles due to hydrogen evolution reaction (HER) or oxygen evolution reaction (OER) are less likely to get trapped beneath the objective lens, disturbing the rays pathway. However, the setup is more complicated if a flow cell is used, as two pumps are necessary to bring the electrolyte in and out. Furthermore, the cell is not closed anymore, making an introduction of air, respectively oxygen, and consequent reactions with the surface or reactants likely. While an optical window in the electrochemical cell provides a safe system, PVC foil attached to the objective is prone to spontaneous irregularities, e.g., fixation and attachment, requiring additional attention. Besides that, it requires water between the objective and foil to have the objective immersed in water.

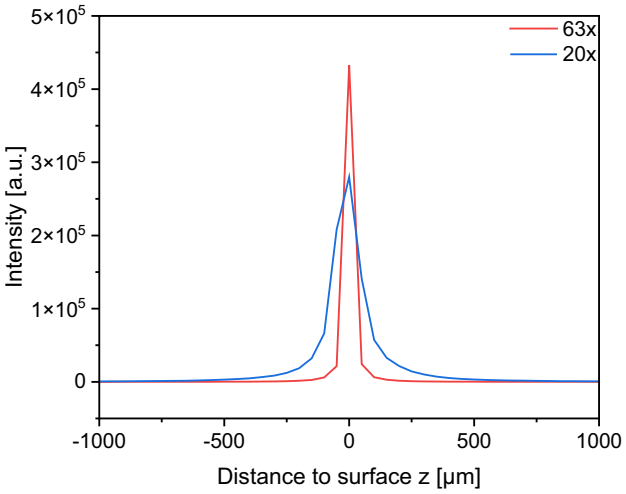

Fig. 8 Comparison of depth profiles of a 20×(NA = 0.5, WD = 3.5 mm) and a 63×(NA = 0.9, WD = 2.2 mm) water immersion objective covered with a PVC foil with z = 0 at the electrode–electrolyte interface with the pyridine ring breathing mode signal intensity [66] at 1008.5 cm^{-1}

Figure 8 shows the results of a 20×(0.5 NA) and a 63×(0.9 NA) water immersion objective performing a depth profile similar to that shown in Fig. 6. As the sapphire-less setup shown in Fig. 7D was employed, $z = 0$ is defined as a focus at the electrode surface. A comparison of the two depth profiles at the same spot reveals that for the 63× magnified objective, a higher intensity was measured while the peak was narrower than for the 20× objective, whereas the 20× water immersion objective exhibits less intense signals and a broader area a considerable signal derives from. This trend nicely shows the critical influence of an objective with a high NA as it aids with higher signal intensity, especially helpful for inherently low intensities or concentrations [62]. Furthermore, a higher NA provides a better spatial resolution.

As the described experiments reveal, the choice of the objective can significantly affect the quality of spectroelectrochemical results. Therefore, it should become good scientific practice to provide respective information on the objective to support reproducibility and awareness of the topic's importance. As there is no optimal objective for all applications, there is always a trade-off between signal intensity, spatial resolution, practicability, and objective price. All in all, for choosing a suitable objective, the immersion medium, numerical aperture, magnification, working distance, and setup are crucial as they can influence the quality of the obtaining spectra.

A delicate aspect that has not been covered in this section but requires attention is the risk of inhomogeneous current density distributions in the cell. It is caused by an obstruction of the current path by too small distances between the objective lens and the electrode surface—especially pronounced at large magnification and when using high NA water immersion objectives.

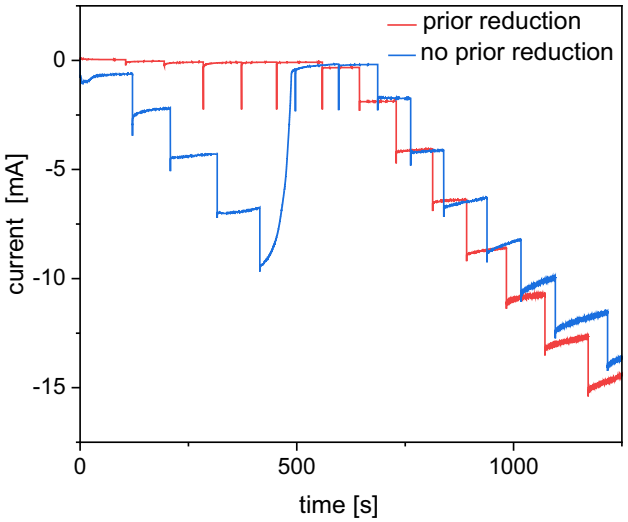

Fig. 9 Comparison of multi-step chronoamperometric measurements with the electrode potential being varied between 0.0 V and −1.3 V (0.1 V steps) for copper working electrodes in 0.1 M H_2SO_4 solution with and without a previous reductive conditioning step

Further influences on the spectra

Besides the existing chance for all Raman spectrometric experiments to detect cosmic rays from ubiquitous radiation, additional potentially problematic signals may arise during electrochemical *in operando* measurements. Thus, depending on the SERS substrate preparation procedure, different additional signals can arise from it. Small amounts of reducing agents or tensides can remain on the SERS substrate, leading to undesired signals for chemically reduced colloids. As SERS is a highly sensitive spectroscopic technique, any impurity from involved chemicals can contribute to observing such signals. Besides electrolyte material and water, one often overlooked contribution can originate from a memory effect of incompatible tube materials when flow-through cells are used. If the SERS effect is generated by ORC, surface oxide species are usually formed with the roughened surface. This implies two consequences, especially for reduction reactions. First, as the metal surface is (at least partially) oxidized, metal oxide signals can considerably contribute to the Raman spectrum and potentially alter the desired Raman spectrum of the examined signals on a metal surface to a Raman spectrum on the respective metal oxide surface. The oxide layer can also dampen the enhancement of the SERS substrate [71]. Secondly, when applying reduction potentials, an electrochemical reduction of the metal oxides leads to currents that are not related to the target reaction of the experiment. These currents are generally characterized by a sudden drop after a complete oxide reduction (Fig. 9, blue curve). Applying a reductive potential to remove the oxide layer prior to the actual measurement solves this issue (Fig. 9, red curve). Alternatively, the use of oxide-dissolving electrolytes like aqueous sulfuric acid can aid.

Furthermore, highly energetic lasers with high intensity or low wavelength can cause photoinduced destruction of the surface structure or destroy analyte molecules. The consequence is a highly damped enhancement and undesired Raman signals of the residuals. Besides choosing the laser intensity as low as possible, these issues can, if necessary, be addressed by varying the illuminated surface area frequently and choosing a flow reactor for a constant exchange of analytes. It is also recommended to reduce the laser intensity in order to avoid temperature-dependent fluctuations [72]. Additionally, the laser can introduce fluorescence, leading to an increased background signal [25].

Furthermore, Raman spectra can be influenced by the electrode potential. The absorption maximum of surface plasmons is potential dependent, leading to differences in their ability to enhance the Raman signal. The potential of zero charge (PZC) can explain another influence [62]. If the amount of positive charges at the electrode surface dominates, the surface will mainly attract negative charges, while a negatively charged electrode surface accumulates positive charges close to the surface. At the PZC, no charge dominates at the electrode surface. At this potential, it comes to a reorientation process of ionic species, solvents, and analyte molecules, implying changes in signal enhancement. More negative or positive potentials can also lead to analytes having a weaker bond to the surface and moving further away. While reorientation can lead to different signals preferentially enhanced with the electromagnetic mechanisms, it can also change the bonding situation, followed by a different

chemical enhancement. The proximity of the analyte to the surface contributes to its intensity. Besides processes in the electrochemical double layer, the SERS effect can decline over time as the roughened metal surface can restructure towards an energetically more favored surface. This restructuring is accelerated at more negative potentials due to the repulsion of anions that stabilize unstable surface facets, while more positive potentials lead to oxidative destruction of the surface and, again, lower enhancement factors [2]. The instability of the SERS substrate results in irreversible electrochemical steps [2]. Also, a dependency of the used laser wavelength was described [66]. The influences of the different enhancement mechanisms, the spatial orientation, the proximity to the electrode surface, and the grade of the roughened surface changes are difficult to distinguish and make an evaluation challenging and signal intensities challenging to correlate [2]. Tian et al. and Wu et al. provide a more in-depth description of electrode/electrolyte interactions interfering with measurements [2, 62].

Further on, the background signal depends on the interaction of substrate and molecule: an electron donation decreases the background, while withdrawal increases the background. This applies to the properties of the adsorbed molecules and the electrode potential [73].

A method to overcome potentially problematic signals due to impurities, strong electrolyte signals, and complex spectra is signal arithmetic. Subtraction of either the Raman spectrum of the electrolyte or, if the potential is varied stepwise, the spectra of consecutive potentials lead to spectra that only show the desired Raman bands, respectively, the reaction to the performed changes [42, 62]. The Raman spectra must be normalized to be subtractable for performing this operation. The information for absolute signal intensity is lost and cannot be compared afterward, while a better relative comparison of the signal intensity changes can be executed [2]. Normalization can also aid in comparing relative intensities for spectra obtained at different potentials with various phenomena causing varying overall intensities [42].

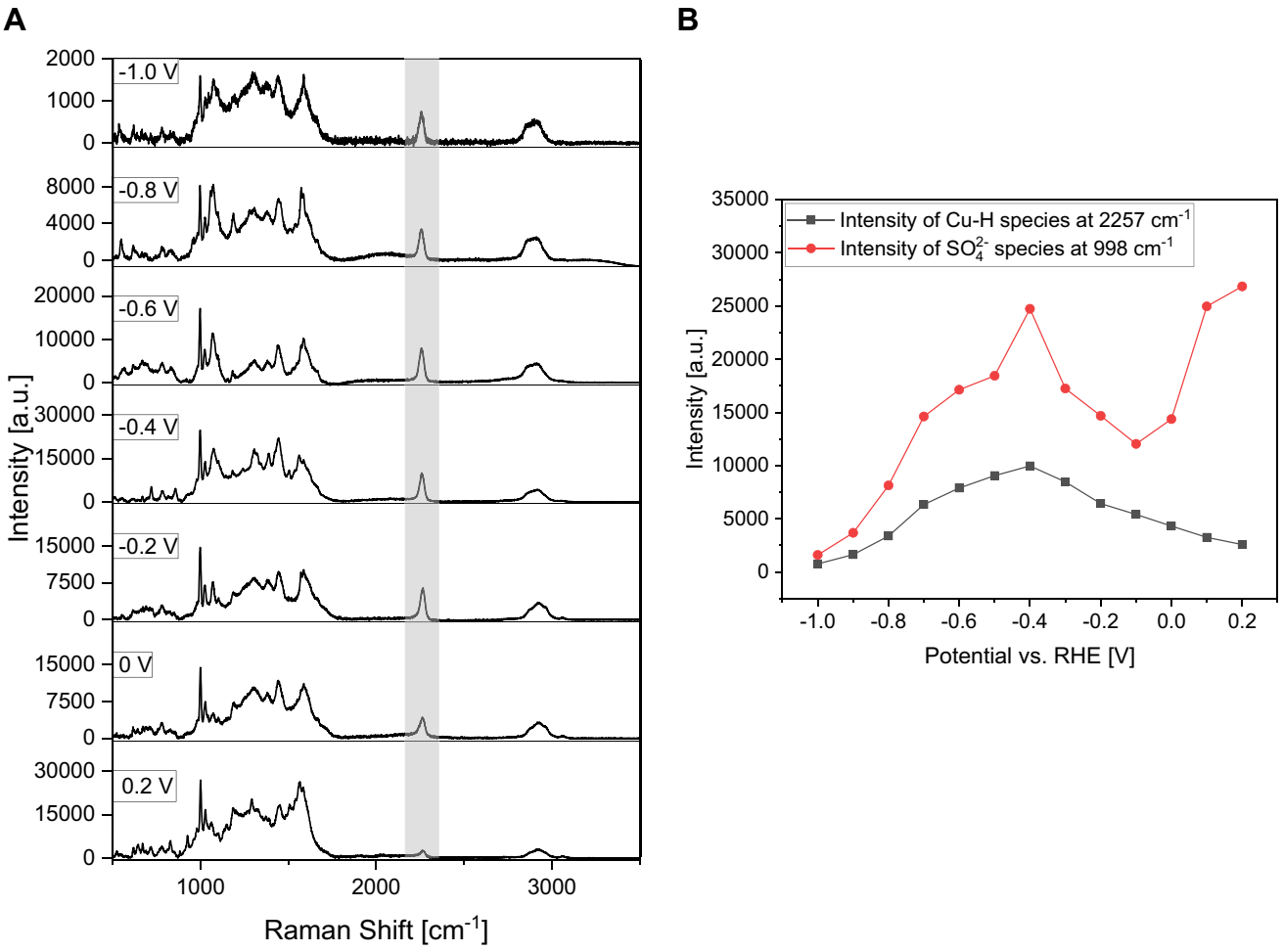

Fig. 10 **A** *In operando* electrochemical Raman experiment on a roughened copper surface with 0.1 M aqueous H_2SO_4 solution, potential altered stepwise: starting at 0.2 V vs. RHE (785 nm laser, 10 s, 1 accumulation, 1% intensity); marked in grey: signal at 2257 cm^{-1}. **B** Potential-dependent intensity of the Cu-H species (2257 cm^{-1}) and SO_4^{2-} (998 cm^{-1})

Essential for an in-depth understanding of phenomena are supporting computational studies like density functional theory (DFT) or molecular dynamics (MD) simulations to estimate Raman shifts and correlating vibrations, orientations, and interactions of surface species [7, 8, 40, 42, 52].

Exemplary considerations: hydride on Cu surface

This section aims to give an example of an *in operando* electrochemical experiment. For this purpose, an electrochemical Raman cell was filled with 0.1 M aqueous H_2SO_4 electrolyte solution after ORC, and a stepwise potential variation from 0.2 V to − 1.0 V was performed (Fig. 10). Several typical vibrations for aqueous sulfuric acid solution in water can be observed [34]. Two observations are discussed here. First, a vibration at 2257 cm^{-1} can be found. Compared to the overall spectrum, it is small at more positive potentials but eventually gains intensity at increasingly negative potentials (Fig. 10B). We attribute this signal to the Cu-H vibration, starting with underpotential deposition and increasing its amount due to an approach towards the hydrogen evolution reaction (HER). The proposed Cu-H vibration is in the same range as the comparable Pt–H vibration described by Tian et al. at 2039–2094 cm^{-1} [15]. Li et al. assigned a weak signal at 2078 cm^{-1} as a Cu-H vibration [74]. Differences can be explained by the different pH values and electrolyte systems. The more acidic 0.1 M H_2SO_4 solution produces a higher hydrogen coverage at the surface, yielding a more pronounced Cu-H signal than the 1 M sulfate solution at pH 3. Second, the overall intensity changes. After its first maximum at 0.2 V, it decreases until it reaches its maximum intensity at a potential of $^{-}$0.4 V and subsequently reduces its overall intensity. This behavior is exemplarily depicted in Fig. 10B by the intensity trend of the SO_4^{2-} signal at 998 cm^{-1}. The first intensity decline and the following intensity maximum can be explained by a mixture of PZC and shifts in plasmon resonance. The subsequent decline of the signal can be attributed to surface restructuring at more negative potentials, accelerated by anion desorption and the anion adsorption itself. A complete intensity and signal interpretation of both background and analyte signals can be complex and, therefore, requires unavailable knowledge to understand them completely [41].

Conclusion

The conduction of *in operando* electrochemical Raman spectroscopy requires the consideration of multiple experimental factors. As Raman scattering has a low portion of scattered light, the signals originating from analyte molecules close to the surface need to be enhanced. SERS provides suitable tools for this enhancement of molecules near the surface. A wide variety of procedures for the generation of SERS substrates is available, giving the opportunity to find a method suitable for the desired experiment. While ORC are easily implemented in electrochemical experiment setups, they are not as homogenous and, therefore, spectra are not as reproducibly intense as other methods. Alternative methods are available and also enable experiments with otherwise not SERS active surfaces. The outcome of a Raman experiment also depends on the utilized laser light, as the intensity of SERS is highly dependent on the interaction between substrate and laser wavelength. If the optimal conditions for the enhancement are found, it is crucial to use the optimal objectives. Water immersion objective lenses with high numerical aperture show higher signal intensity and spatial resolution with fewer aberrations than metallurgical objective lenses. Several surface phenomena will affect the resulting surface spectra if the experimental setup is fully optimized. Depending on the charge and potential at the surface, signal intensity can vary, but also spectra can change due to reorientation and restructuring of the electrochemical double layer. Both challenge and opportunity for *in operando* electrochemical Raman spectroscopy lie in these electrochemical double-layer changes. If interpreted correctly, they can provide information on the molecule's orientation, proximity, and interaction with the electrode. In order to fully use this potential of the method and avoid misinterpretations, there has to be a complete understanding of the fundamental processes.

Experimental

In the executed experiments, an InVIA Reflex Raman confocal microscope (Renishaw plc, UK) equipped with a 532 nm (Nd:Yag, 50 mW) and a 785 nm (diode, 300 mW) laser was used, employing its confocal mode. An internal silicon reference was used for a spectral calibration at 520.5 cm^{-1}. Data acquisition, cosmic ray removal, and background subtraction were accomplished with the WiRe 5.0 Software (Renishaw plc, UK). If not stated otherwise, the confocal microscope was equipped with a water immersion objective (HCX APO L 20×, 0.5 NA W U-V-I-/D 3.5, Leica Microsystems, Germany). For comparison, experiments with a metallurgical objective (N PLAN 5×, 0.12 NA, Leica Microsystems, Germany) and a water immersion objective (HC APO L 63×, 0.9 NA W U-V-I CS2, Leica Microsystems, Germany) were performed. The electrochemical cell was a Raman Electrochemical Flow Cell (Redox.Me, Sweden) with a volume of 4.5 mL and an electrode area of 3.5 cm^2 in contact with the solution. Copper (99.995%, ChemPUR, Germany) and silver (99.995%, ChemPUR, Germany) foils, 0.5 mm thick,

were used as working electrodes, while a 0.6 mm thick and 150 mm long platinum wire (99.9%, Redox.Me, Sweden) was used as the counter electrode. The reference electrode was a 3 M NaCl Ag|AgCl electrode (RE-1B, BioLogic, France). All potentials are referenced vs. reversible hydrogen electrode (RHE) if not stated otherwise. The potentials and currents at the electrodes were adjusted and measured with an SP-150 Potentiostat (BioLogic SAS, France). Silver and copper electrodes were polished prior to use. For this purpose, they were ground with abrasive paper (2400 and 12,000), polishing diamond (1 µm), and polishing alumina (0.05 µm) to start with a uniform smooth surface. Copper electrodes were roughened using ORC in 0.1 M KCl without an electrolyte flow. After the electrolyte solution was filled in, it was stopped, and the potential cycled 20 times between –0.2 V and 0.9 V vs. Ag|AgCl with a sweep rate of 20 mV/s. Silver electrodes were roughened using another ORC procedure in 0.1 M KCl solution [75]. After the ORC, the electrolyte was exchanged with an electrolyte and analyte solution of interest. Typical flow rates of 1.00 mL/min were achieved with an Ismatec Reglo Digital peristaltic pump (Cole-Parmer, USA) combined with Viton and PTFE tubes. For in situ electrochemical experiments with stepwisely changed electrode potential, conditioning was performed prior to the measurements at − 0.2 V vs. Ag|AgCl until the oxide layer was reduced. The completion of the reduction reaction was reached when the measurement current dropped to ca. 0 mA. 0.1 M KCl solutions employed for ORC were prepared from bidestilled water (Carl Roth, Germany) and KCl (99%, Carl Roth, Germany). 0.1 M aqueous sulfuric acid solutions were prepared with suprapur sulfuric acid (96%, Sigma Aldrich, Germany). 0.05 M pyridine solutions were made with anhydrous pyridine (99.8%, Sigma Aldrich, Germany).

Images of the surface morphology were obtained with a Zeiss Evo SEM (Carl Zeiss AG, Germany).

Acknowledgements The authors acknowledge the funding by the Deutsche Forschungsgemeinschaft (DFG, German Research Foundation) under Germany's Excellence Strategy EXC 2163-1 – Sustainable and Energy Efficient Aviation – Project ID 390881007. The authors also acknowledge support by the DFG Major Instrumentation Program (INST 188 / 420-1 FUGG).

Funding Open Access funding enabled and organized by Projekt DEAL.

Declarations

Conflict of interest The authors declare no competing interests.

References

1. Zhu Y, Wang J, Chu H et al (2020) In situ/ operando studies for designing next-generation electrocatalysts. ACS Energy Lett 5:1281–1291. https://doi.org/10.1021/acsenergylett.0c00305
2. Tian ZQ, Ren B (2004) Adsorption and reaction at electrochemical interfaces as probed by surface-enhanced Raman spectroscopy. Annu Rev Phys Chem 55:197–229. https://doi.org/10.1146/annurev.physchem.54.011002.103833
3. McKenzie ECR, Hosseini S, Petro AGC et al (2022) Versatile tools for understanding electrosynthetic mechanisms. Chem Rev 122:3292–3335. https://doi.org/10.1021/acs.chemrev.1c00471
4. Hess C (2021) New advances in using Raman spectroscopy for the characterization of catalysts and catalytic reactions. Chem Soc Rev 50:3519–3564. https://doi.org/10.1039/d0cs01059f
5. Wachs IE, Roberts CA (2010) Monitoring surface metal oxide catalytic active sites with Raman spectroscopy. Chem Soc Rev 39:5002–5017. https://doi.org/10.1039/c0cs00145g
6. Stavitski E, Weckhuysen BM (2010) Infrared and Raman imaging of heterogeneous catalysts. Chem Soc Rev 39:4615–4625. https://doi.org/10.1039/c0cs00064g
7. Lenk T, Rabet S, Sprick M et al (2022) Insight into the interaction of furfural with metallic surfaces in the electrochemical hydrogenation process, from *in operando* Raman spectroscopy and molecular dynamics simulations. Chem Phys Chem. https://doi.org/10.1002/cphc.202200614
8. Wang A, Huang YF, Sur UK et al (2010) In situ identification of intermediates of benzyl chloride reduction at a silver electrode by SERS coupled with DFT calculations. J Am Chem Soc 132:9534–9536. https://doi.org/10.1021/ja1024639
9. Ibañez D, Santidrian A, Heras A et al (2015) Study of adenine and guanine oxidation mechanism by surface-enhanced Raman spectroelectrochemistry. J Phys Chem C 119:8191–8198. https://doi.org/10.1021/acs.jpcc.5b00938
10. Heidary N, Kornienko N (2020) Electrochemical biomass valorization on gold-metal oxide nanoscale heterojunctions enables investigation of both catalyst and reaction dynamics with: operando surface-enhanced Raman spectroscopy. Chem Sci 11:1798–1806. https://doi.org/10.1039/d0sc00136h
11. Heidary N, Kornienko N (2019) Operando Raman probing of electrocatalytic biomass oxidation on gold nanoparticle surfaces. Chem Commun 55:11996–11999. https://doi.org/10.1039/c9cc06646b
12. Li X, Gewirth AA (2005) Oxygen electroreduction through a superoxide intermediate on Bi-modified Au surfaces. J Am Chem Soc 127:5252–5260. https://doi.org/10.1021/ja043170a
13. Deng Y, Handoko AD, Du Y et al (2016) In situ Raman spectroscopy of copper and copper oxide surfaces during electrochemical oxygen evolution reaction: identification of CuIII oxides as catalytically active species. ACS Catal 6:2473–2481. https://doi.org/10.1021/acscatal.6b00205
14. Schlüter N, Novák P, Schröder D (2022) Nonlinear electrochemical analysis: worth the effort to reveal new insights into energy materials. Adv Energy Mater 2200708:2200708. https://doi.org/10.1002/aenm.202200708
15. Tian ZQ, Ren B, Chen YX et al (1996) Probing electrode/electrolyte interfacial structure in the potential region of hydrogen evolution by Raman spectroscopy. J Chem Soc Faraday Trans 92:3829–3838. https://doi.org/10.1039/ft9969203829

16. Ogino SI, Itoh T, Mabuchi D et al (2016) In situ electrochemical Raman spectroscopy of air-oxidized semiconducting single-walled carbon nanotube bundles in aqueous sulfuric acid solution. J Phys Chem C 120:7133–7143. https://doi.org/10.1021/acs.jpcc.5b12057
17. Fleger Y, Mastai Y, Rosenbluh M, Dressler DH (2009) SERS as a probe for adsorbate orientation on silver nanoclusters. J Raman Spectrosc 40:1572–1577. https://doi.org/10.1002/jrs.2300
18. Meyer L, Saqib N, Porter J (2021) Review—operando optical spectroscopy studies of batteries. J Electrochem Soc 168:090561. https://doi.org/10.1149/1945-7111/AC2088
19. Raman CV, Krishnan KS (1928) A new type of secondary radiation. Nature 121:501–502. https://doi.org/10.1038/121501c0
20. Vandenabeele P (2013) Practical Raman spectroscopy-an introduction. John Wiley & Sons Ltd, Chichester
21. Orlando A, Franceschini F, Muscas C et al (2021) A comprehensive review on Raman spectroscopy applications. Chemosensors 9:1–28. https://doi.org/10.3390/chemosensors9090262
22. Colthup NC, Daly L, Wiberley S (1990) Introduction to infrared and Raman spectroscopy, 3rd edn. Academic Press, New York
23. Li S, Li Y, Yi R et al (2020) Coherent anti-Stokes Raman scattering microscopy and its applications. Front Phys 8:1–9. https://doi.org/10.3389/fphy.2020.598420
24. Diem M (2015) *Modern vibrational spectroscopy and micro-spectroscopy*. John Wiley & Sons Ltd, West Sussex
25. Mestl G (2000) In situ Raman spectroscopy - a valuable tool to understand operating catalysts. J Mol Catal A Chem 158:45–65. https://doi.org/10.1016/S1381-1169(00)00042-X
26. Schrader B (1973) Chemical applications of Raman spectroscopy. Angew Chem Int Ed 12:884–908. https://doi.org/10.1002/anie.197308841
27. Wang HL, You EM, Panneerselvam R et al (2021) Advances of surface-enhanced Raman and IR spectroscopies: from nano/microstructures to macro-optical design. Light Sci Appl 10. https://doi.org/10.1038/s41377-021-00599-2
28. Anibal J, Xu B (2020) Electroreductive C-C coupling of furfural and benzaldehyde on Cu and Pb surfaces. ACS Catal 10:11643–11653. https://doi.org/10.1021/acscatal.0c03110
29. Román AM, Hasse JC, Medlin JW, Holewinski A (2019) Elucidating acidic electro-oxidation pathways of furfural on platinum. ACS Catal 9:10305–10316. https://doi.org/10.1021/acscatal.9b02656
30. Yao Y, Zhu S, Wang H et al (2020) A spectroscopic study of electrochemical nitrogen and nitrate reduction on rhodium surfaces. Angew Chemie Int Ed 59:10479–10483. https://doi.org/10.1002/anie.202003071
31. Lin Y, Liu Z, Yu L et al (2021) Overall oxygen electrocatalysis on nitrogen-modified carbon catalysts: identification of active sites and in situ observation of reactive intermediates. Angew Chem Int Ed 60:3299–3306. https://doi.org/10.1002/anie.202012615
32. Das RS, Agrawal YK (2011) Raman spectroscopy: recent advancements, techniques and applications. Vib Spectrosc 57:163–176. https://doi.org/10.1016/j.vibspec.2011.08.003
33. Tian ZQ, Ren B, Wu DY (2002) Surface-enhanced Raman scattering: from noble to transition metals and from rough surfaces to ordered nanostructures. J Phys Chem B 106:9463–9483. https://doi.org/10.1021/jp0257449
34. Lund Myhre CE, Christensen DH, Nicolaisen FM, Nielsen CJ (2003) Spectroscopic study of aqueous H2SO4 at different temperatures and compositions: variations in dissociation and optical properties. J Phys Chem A 107:1979–1991. https://doi.org/10.1021/jp026576n
35. Kudelski A, Janik-Czachor M, Bukowska J et al (1999) Surface-enhanced Raman scattering (SERS) on copper electrodeposited under nonequilibrium conditions. J Mol Struct 482–483:245–248. https://doi.org/10.1016/S0022-2860(98)00664-4
36. Zuo C, Jagodzinski PW (2005) Surface-enhanced raman scattering of pyridine using different metals: differences and explanation based on the selective formation of α-pyridyl on metal surfaces. J Phys Chem B 109:1788–1793. https://doi.org/10.1021/jp0406363
37. Halvorson RA, Vikesland PJ (2010) Surface-enhanced Raman spectroscopy (SERS) for environmental analyses. Environ Sci Technol 44:7749–7755. https://doi.org/10.1021/es101228z
38. Fan M, Andrade GFS, Brolo AG (2011) A review on the fabrication of substrates for surface enhanced Raman spectroscopy and their applications in analytical chemistry. Anal Chim Acta 693:7–25. https://doi.org/10.1016/j.aca.2011.03.002
39. Bonifacio A, Cervo S, Sergo V (2015) Label-free surface-enhanced Raman spectroscopy of biofluids: fundamental aspects and diagnostic applications. Anal Bioanal Chem 407:8265–8277. https://doi.org/10.1007/s00216-015-8697-z
40. Langer J, de Aberasturi DJ, Aizpurua J et al (2020) Present and future of surface-enhanced Raman scattering. ACS Nano 14:28–117. https://doi.org/10.1021/acsnano.9b04224
41. Schlücker S (2014) Surface-enhanced raman spectroscopy: concepts and chemical applications. Angew Chem Int Ed 53:4756–4795. https://doi.org/10.1002/anie.201205748
42. Han XX, Rodriguez RS, Haynes CL et al (2021) Surface-enhanced Raman spectroscopy. Nat Rev Methods Prim 1:87. https://doi.org/10.1038/s43586-021-00083-6
43. Pérez-Jiménez AI, Lyu D, Lu Z et al (2020) Surface-enhanced Raman spectroscopy: benefits, trade-offs and future developments. Chem Sci 11:4563–4577. https://doi.org/10.1039/d0sc00809e
44. Fleischmann M, Hendra PJ, McQuillan AJ (1974) Raman spectra of pyridine adsorbed at a silver electrode. Chem Phys Lett 26:163–166. https://doi.org/10.1016/0009-2614(74)85388-1
45. Jeanmaire DL, van Duyne RP (1977) Surface Raman spectroelectrochemistry part1. Heterocyclic J Electroanal Chem 84:1
46. Albrecht MG, Creighton JA (1977) Anomalously Intense Raman spectra of pyridine at a silver electrode. J Am Chem Soc 99:5215–5217
47. Le Ru EC, Blackie E, Meyer M, Etchegoint PG (2007) Surface enhanced raman scattering enhancement factors: a comprehensive study. J Phys Chem C 111:13794–13803. https://doi.org/10.1021/jp0687908
48. Hutter E, Fendler JH (2004) Exploitation of localized surface plasmon resonance. Adv Mater 16:1685–1706. https://doi.org/10.1002/adma.200400271
49. Kelly KL, Coronado E, Zhao LL, Schatz GC (2003) The optical properties of metal nanoparticles: the influence of size, shape, and dielectric environment. J Phys Chem B 107:668–677. https://doi.org/10.1080/00094056.2009.10521700
50. Hallmark VM, Campion A (1986) Selection rules for surface Raman spectroscopy: experimental results. J Chem Phys 84:2933–2941. https://doi.org/10.1063/1.450274
51. Moskovits M (1982) Surface selection rules. J Chem Phys 77:4408–4416. https://doi.org/10.1063/1.444442
52. Le Ru ECL, Meyer SA, Artur C et al (2011) Experimental demonstration of surface selection rules for SERS on flat metallic surfaces. Chem Commun 47:3903–3905. https://doi.org/10.1039/c1cc10484e
53. Markin AV, Markina NE, Popp J, Cialla-May D (2018) Copper nanostructures for chemical analysis using surface-enhanced Raman spectroscopy. Trends Anal Chem 108:247–259. https://doi.org/10.1016/j.trac.2018.09.004
54. Sharma B, Frontiera RR, Henry AI et al (2012) SERS: Materials, applications, and the future. Mater Today 15:16–25. https://doi.org/10.1016/S1369-7021(12)70017-2
55. Tian ZQ, Ren B, Li JF, Yang ZL (2007) Expanding generality of surface-enhanced Raman spectroscopy with borrowing SERS activity strategy. Chem Commun 3514–3534. https://doi.org/10.1039/b616986d

56. Li JF, Huang YF, Ding Y et al (2010) Shell-isolated nanoparticle-enhanced Raman spectroscopy. Nature 464:392–395. https://doi.org/10.1038/nature08907
57. Kuruvinashetti K, Zhang Y, Li J, Kornienko N (2020) Shell isolated nanoparticle enhanced Raman spectroscopy for renewable energy electrocatalysis. New J Chem 44:19953–19960. https://doi.org/10.1039/d0nj03526b
58. Kudelski A, Bukowska J, Janik-Czachor M et al (1998) Characterization of the copper surface optimized for use as a substrate for surface-enhanced Raman scattering. Vib Spectrosc 16:21–29. https://doi.org/10.1016/S0924-2031(97)00049-0
59. Panneerselvam R, Xiao L, Waites KB et al (2018) A rapid and simple chemical method for the preparation of Ag colloids for surface-enhanced Raman spectroscopy using the Ag mirror reaction. Vib Spectrosc 98:1–7. https://doi.org/10.1016/j.vibspec.2018.06.011
60. Miller SK, Baiker A, Meier M, Wokaun A (1984) Surface-enhanced Raman scattering and the preparation of copper substrates for catalytic studies. J Chem Soc Faraday Trans 1 Phys Chem Condens Phases 80:1305–1312. https://doi.org/10.1039/F19848001305
61. Cejkova J, Prokopec V, Brazdova S et al (2009) Characterization of copper SERS-active substrates prepared by electrochemical deposition. Appl Surf Sci 255:7864–7870. https://doi.org/10.1016/j.apsusc.2009.04.152
62. Wu DY, Li JF, Ren B, Tian ZQ (2008) Electrochemical surface-enhanced Raman spectroscopy of nanostructures. Chem Soc Rev 37:1025–1041. https://doi.org/10.1039/b707872m
63. Pockrand I (1982) Raman spectroscopy of pyridine-exposed Ag, Cu, and Au films in UHV a comparative study. Chem Phys Lett 85:37–42
64. Giridhar G, Manepalli RRKN, Apparao G (2017) Confocal Raman spectroscopy. In: Spectroscopic methods for nanomaterials characterization. Elsevier Inc., pp 141–161
65. Everall NJ (2010) Confocal Raman microscopy: common errors and artefacts. Analyst 135:2512–2522. https://doi.org/10.1039/c0an00371a
66. Ingram JC, Pemberton JE (1992) Comparison of charge transfer enhancement in the surface enhanced Raman scattering of pyridine on copper and silver electrodes. Langmuir 8:2034–2039. https://doi.org/10.1021/la00044a026
67. Haynes WM (2016) CRC Handbook of chemistry and physics, 97th editi. CRC Press LLC, Boca Raton
68. Everall N (2004) Depth profiling with confocal part II. Spectroscopy 19:16–24
69. Boldrini B, Ostertag E, Rebner K, Oelkrug D (2021) Exploring the hidden depth by confocal Raman experiments with variable objective aperture and magnification. Anal Bioanal Chem 413:7093–7106. https://doi.org/10.1007/s00216-021-03678-w
70. Bott-Neto JL, Rodrigues MVF, Silva MC et al (2020) Versatile spectroelectrochemical cell for in situ experiments: development, applications, and electrochemical behavior. Chem Electro Chem 1–9. https://doi.org/10.1002/celc.202000910
71. Wang RC, Li CH (2011) Cu, Cu-Cu2O core-shell, and hollow Cu2O nanodendrites: structural evolution and reverse surface-enhanced Raman scattering. Acta Mater 59:822–829. https://doi.org/10.1016/j.actamat.2010.10.029
72. Merlen A, Pardanaud C, Gratzer K et al (2020) Spectral fluctuation in SERS spectra of benzodiazepin molecules: the case of oxazepam. J Raman Spectrosc 51:2192–2198. https://doi.org/10.1002/jrs.5972
73. Mahajan S, Cole RM, Speed JD et al (2010) Understanding the surface-enhanced Raman spectroscopy " background." J Phys Chem C 114:7242–7250. https://doi.org/10.1021/jp907197b
74. Li J, Kornienko N (2021) Probing electrosynthetic reactions with furfural on copper surfaces. Chem Commun 57:5127–5130. https://doi.org/10.1039/d1cc01429c
75. Gao P, Gosztola D, Leung LWH, Weaver MJ (1987) Surface-enhanced Raman scattering at gold electrodes: dependence on electrochemical pretreatment conditions and comparisons with silver. J Electroanal Chem 233:211–222. https://doi.org/10.1016/0022-0728(87)85017-9
76. Weckhuysen BM (2003) Determining the active site in a catalytic process: operando spectroscopy is more than a buzzword. Phys Chem Chem Phys 5:4351–4360. https://doi.org/10.1039/b309650p
77. Harnisch F, Schröder U (2019) Tapping renewables: a new dawn for organic electrosynthesis in aqueous reaction media. Chem Electro Chem 6:4126–4133. https://doi.org/10.1002/celc.201900456

Thorben Lenk is a PhD student in the group of Uwe Schröder at TU Braunschweig (Germany). He earned his M.Sc. in chemistry in 2019 with a thesis on inorganic chemistry at the Carl-von-Ossietzky University Oldenburg (Germany), supported by a scholarship from the German Academic Scholarship Foundation (Studienstiftung des deutschen Volkes). During his studies, he completed a research internship at the University of Calgary (Canada). His PhD research focuses on the mechanism of electrochemical synthesis of potential biofuels within the Cluster of Excellence SE2A – Sustainable and Energy Efficient Aviation under German universities' excellence strategy.

Uwe Schröder studied chemistry at Humboldt-University in Berlin, where he obtained his Diploma degree in Analytical Chemistry 1995 and his PhD in Physical Chemistry in 2000. After a postdoctoral stay at Oxford University's Physical and Theoretical Chemistry lab as a Feodor Lynen Fellow, he work at the University of Greifswald, Germany, where he finished his Habilitation in Environmental Chemistry in 2007. In 2008 he was appointed as Chair for Sustainable Chemistry and Energy Research at the Institute of Ecological Chemistry, TU Braunschweig. He was director of this institute from 20152021. In 2021 he appointed chair of Electrobiochemistry at the Institute of Biochemistry, University of Greifswald. Major research interests are, e.g., fundamental and applied aspects of microbial electrochemistry and electrosynthesis.